

# Catalysis Science & Technology

Accepted Manuscript



This is an *Accepted Manuscript*, which has been through the Royal Society of Chemistry peer review process and has been accepted for publication.

*Accepted Manuscripts* are published online shortly after acceptance, before technical editing, formatting and proof reading. Using this free service, authors can make their results available to the community, in citable form, before we publish the edited article. We will replace this *Accepted Manuscript* with the edited and formatted *Advance Article* as soon as it is available.

You can find more information about *Accepted Manuscripts* in the [Information for Authors](#).

Please note that technical editing may introduce minor changes to the text and/or graphics, which may alter content. The journal's standard [Terms & Conditions](#) and the [Ethical guidelines](#) still apply. In no event shall the Royal Society of Chemistry be held responsible for any errors or omissions in this *Accepted Manuscript* or any consequences arising from the use of any information it contains.

## PERSPECTIVE

## Applications of Yttria Stabilized Zirconia (YSZ) in catalysis

M. N. Tsampas,<sup>a</sup> F. M. Sapountzi,<sup>b</sup> and P. Vernoux<sup>b</sup>Received 00th January 20xx,  
Accepted 00th January 20xx

DOI: 10.1039/x0xx00000x

www.rsc.org/

This article describes recent advances in the use of Yttria Stabilized Zirconia (YSZ), an oxygen ion conductor, for catalytic applications. This ceramic material combines different functionalities such as a good thermal stability, a selective bulk oxygen mobility and a high surface oxygen vacancies concentration. These properties have been first exploited, as dense membranes, in the field of solid oxide fuel cells and electrochemical promotion of catalysis. More recently, YSZ, as nanometric powders, is also considered as a promising support for metallic nanoparticles or as a catalyst itself. This paper summarizes the main applications of YSZ in the aforementioned fields, explains the underlying phenomena and finally gives perspectives for future applications of YSZ.

## 1. Introduction

Ceramic oxygen-ion conductors (or solid electrolytes) are of the most common anionic conducting ceramics involved in heterogeneous catalysis<sup>1</sup>. Their use in heterogeneous catalysis was first proposed in 1970 by Wagner<sup>2</sup>, who suggested the use of solid electrolyte cells for the measurement of oxygen activity on metal and metal oxide catalysts. Few years later, this technique was implemented for the investigation of the mechanism of SO<sub>2</sub> oxidation on noble metals<sup>3</sup> and was subsequently called solid electrolyte potentiometry (SEP)<sup>4</sup>. Since 1980, the use of oxygen ion conductors in heterogeneous catalysis has been extended and O<sup>2-</sup> conductors have found numerous applications:

- for electrochemically supplying (a) either reactant oxygen for a catalytic oxidation reaction<sup>5</sup>, (b) or promoting oxygen ions to catalytic films in order to improve the activity and/or the selectivity<sup>6</sup>,
- as active catalytic carriers for highly dispersed metallic nanoparticles, promoting the catalytic activity or limiting the poisoning of active sites<sup>1</sup>,
- as catalysts such as for the partial oxidation of methane.

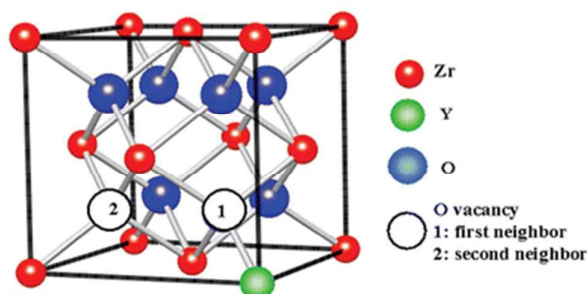
The movement of oxide ions through the crystal lattice of oxygen ion conductors results of thermally-activated hopping, moving from one crystal lattice site to another, with a superimposed drift in the direction of the electric field<sup>7</sup>.

The most conventional fast oxide-ion conducting materials have fluorite type crystal structure, AO<sub>2</sub>, where A is a tetravalent cation<sup>8</sup>. In this structure, the cations occupy face-

centred positions in a cubic unit cell with anions in the eight tetrahedral

sites between them. The general formula of a fluorite structure is AO<sub>2</sub>, where A is a large tetravalent cation (Zr, U, Th, Ce)<sup>7,8</sup>.

The best known fluorite-type oxide-ion conductor is acceptor doped ZrO<sub>2</sub>. Pure zirconia (ZrO<sub>2</sub>) has poor ionic conductivity, and only adopts the cubic fluorite symmetry above 2300°C<sup>7,9</sup>. To stabilize the cubic structure at lower temperatures and to increase the concentration of oxygen vacancies (which are required for ionic conduction via vacancy hopping), doping is usually performed by introducing acceptor dopants into the cation sublattice<sup>7,10,11</sup>. Doping of the fluorite oxides is usually achieved by substitution of the host cation with either a rare earth or an alkaline earth<sup>12</sup>, as shown in Figure 1. Typical



subvalent dopants (i.e. acceptors) are Y<sup>3+</sup> and Ca<sup>2+</sup>, producing yttria-stabilized zirconia (YSZ) and calcia-stabilized zirconia (CSZ) respectively.

**Figure 1:** Defect fluorite structure, as in Yttria Stabilized Zirconia. Reprinted from ref. 12 with the permission of RSC.

YSZ is a material with unique characteristics and enhanced chemical stability compared to other ceramic conductors. YSZ can maintain a stable cubic fluorite structure between room temperature and 2700°C, while it exhibits extremely low

<sup>a</sup> Dutch Institute For Fundamental Energy Research, 5612 AJ Eindhoven, The Netherlands

<sup>b</sup> Université de Lyon, Institut de Recherches sur la Catalyse et l'Environnement de Lyon, UMR 5256, CNRS, Université Claude Bernard Lyon 1, 2 avenue A. Einstein, 69626 Villeurbanne, France.

thermal conductivity at high temperatures and considerable high oxygen ionic conductivity<sup>13,14</sup>. Y substitutions of 8-10 mol% show the highest conductivities at temperatures above 800°C. At higher dopant concentrations, the ionic conductivity is limited<sup>7</sup>.

YSZ is the most common oxygen ion conductive electrolyte used in Solid Oxide Fuel Cells<sup>15</sup> and in gas sensors<sup>16</sup>. Apart from its applications in the field of electrocatalysis, YSZ has been extensively used as electrolytic support in catalytic applications using solid electrolyte cell reactors as well as in the frame of the phenomenon of Electrochemical Promotion of Catalysis (EPOC)<sup>6</sup>. Moreover, in the last decades, there is a growing interest in using YSZ in conventional catalytic systems, either as a catalyst itself or as the carrier for metallic nanoparticles. The aim of the present article is to give an insight of these different applications of YSZ in heterogeneous catalysis, mainly focusing on recent studies performed by the authors of this manuscript. Future perspectives and the impact of these studies on the development of smart and efficient catalysts are also discussed.

## 2. YSZ as an electrolytic support: Electrochemical Promotion of Catalysis (EPOC)

### 2.1. Phenomenology

The phenomenon of electrochemical promotion of catalytic activity (EPOC) or non-Faradaic electrochemical modification of catalytic activity (NEMCA) effect refers to the pronounced, reversible and controlled changes in catalytic properties (activity and selectivity) of an electrochemical catalyst (an electronically conducting layer of catalyst interfaced with an electrolytic membrane) observed upon electrical polarizations<sup>1,6,17,18</sup>.

Since the discovery of the effect in the early 80s by Stoukides and Vayenas<sup>19</sup>, more than 100 different catalytic systems (oxidations, hydrogenations, dehydrogenations, isomerizations, decompositions) have been electrochemically promoted on various metal catalysts supported on different ionic conductors. The majority of these studies has been performed with YSZ as the electrolyte<sup>1,6,17,18</sup>.

The basic phenomenology of EPOC when using O<sup>2-</sup> conducting supports is given in figure 2. The (usually porous) metal catalyst-electrode (Pt in the case of figure 2a), typically 40 nm to 4 μm thick, is deposited on an 8 mol% Y<sub>2</sub>O<sub>3</sub>-stabilized-ZrO<sub>2</sub> (YSZ) solid electrolyte. The reactants are co-fed over the porous electrochemical catalytic layer (or conductive porous catalytic layer) (e.g. CO, C<sub>3</sub>H<sub>8</sub> oxidation on Pt), which simultaneously serves as the working electrode in a solid electrolyte cell (figure 2a). Application of an electrical current (1-100 μA/cm<sup>2</sup>) or potential (±2 V) between the catalyst and a counter electrode deposited on the opposite side of the electrolyte, causes pronounced and reversible non-Faradaic alterations of the catalytic reaction rate<sup>1,6,17,18</sup>.

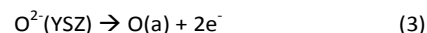
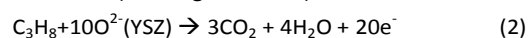
At open circuit conditions on the catalyst electrode (top) an heterogeneous catalytic reaction (no net charge-transfer), i.e. C<sub>3</sub>H<sub>8</sub> oxidation, is taking place with a rate, r<sub>oc</sub> (denoted as r<sub>oc</sub> for Open Circuit). Upon varying the potential of the catalyst

electrode, U<sub>WR</sub>, the cell current, I, is also varied. This current is related to the electrocatalytic (net-charge transfer) reaction rate, r<sub>el</sub>, which is directly proportional to the current, according to the Faraday's law (1).

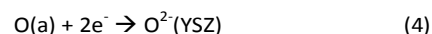
$$r_{el} = I/nF \quad (1)$$

where F is the Faraday's constant and n is the number of electrons involved in the electrochemical reaction. For the case of YSZ, the electrochemical reactions taking place at the catalyst/solid electrolyte/gas three-phase-boundaries (tpb) are:

(working electrode)



(counter electrode)



where O(a) denotes atomic oxygen adsorbed on the catalyst surface. If all the oxygen ions arriving at the top electrode reacts with C<sub>3</sub>H<sub>8</sub>, the maximal rate of C<sub>3</sub>H<sub>8</sub> electro-oxidation is equal to r<sub>el</sub>. Thus, in the experimental setup of EPOC (figure 2), one can expect that upon polarization, the rate of the C<sub>3</sub>H<sub>8</sub> oxidation (denoted as r<sub>pr</sub> for promotion) will be at maximum the sum of the catalytic and electrocatalytic rates, r<sub>pr</sub>=r<sub>oc</sub>+r<sub>el</sub> (=r<sub>oc</sub>+I/nF). On the opposite side, the rate increase, Δr=r<sub>pr</sub>-r<sub>oc</sub> can exceed r<sub>el</sub> (=I/nF) by several orders of magnitude, depending on the experimental conditions.

This is clearly shown in figure 2b, which presents the rate of CO<sub>2</sub> production in the frame of EPOC. At open circuit conditions (i=0), the average reaction rate is equal to 21.4 nmol O/s. Application of a positive current (t=0) leads to migration of oxygen ions onto the catalyst surface. These ionic species act as promoters, thus a 7-fold increase of the catalytic rate is obtained. This enhancement of the catalytic activity is 257 times higher than that predicted by the Faraday's law. In addition, this phenomenon is reversible as upon current interruption (t=30min) the rate gradually returns to its initial value in a short period of time equal with the promoters lifetime (Figure 2).

In order to describe the magnitude of the effect two parameters are commonly used<sup>1,6</sup>.

(i) First, the apparent Faradaic efficiency, Λ, defined from:

$$\Lambda = (r_{pr} - r_{oc}) / (I/nF) = \Delta r / (I/nF) \quad (5)$$

A reaction exhibits electrochemical promotion when |Λ|>1, while electrocatalysis is limited to |Λ|≤1. A reaction is termed electrophobic when Λ>1 (which means that the rate increases with catalyst potential, U<sub>WR</sub>) and electrophilic when Λ<-1 (which means that the rate decreases with catalyst potential, U<sub>WR</sub>). Values of the Faradaic efficiency up to 10<sup>5</sup> have been found in solid state electrochemistry and up to 10<sup>2</sup> in aqueous electrochemistry<sup>6</sup>. In the example of figure 2, the Faradaic efficiency is equal to 257. This underlines that the magnitude of electrochemical activation is much higher than that predicted by Faraday's law. Therefore, EPOC requires low currents or potentials so minimal electrical energy is consumed. Moreover, promoting species such as O<sup>2-</sup> cannot be

formed via gaseous adsorption and cannot be easily dosed by chemical ways.

(ii) Second, the rate enhancement ratio,  $\rho$ , defined from:

$$\rho = r_{pr} / r_{oc} \quad (6)$$

$\rho$  values up to 150<sup>6</sup> have been found for several systems (more recently  $\rho$  values between 300 and 1200<sup>21,22</sup> have been measured).

## PERSPECTIVE

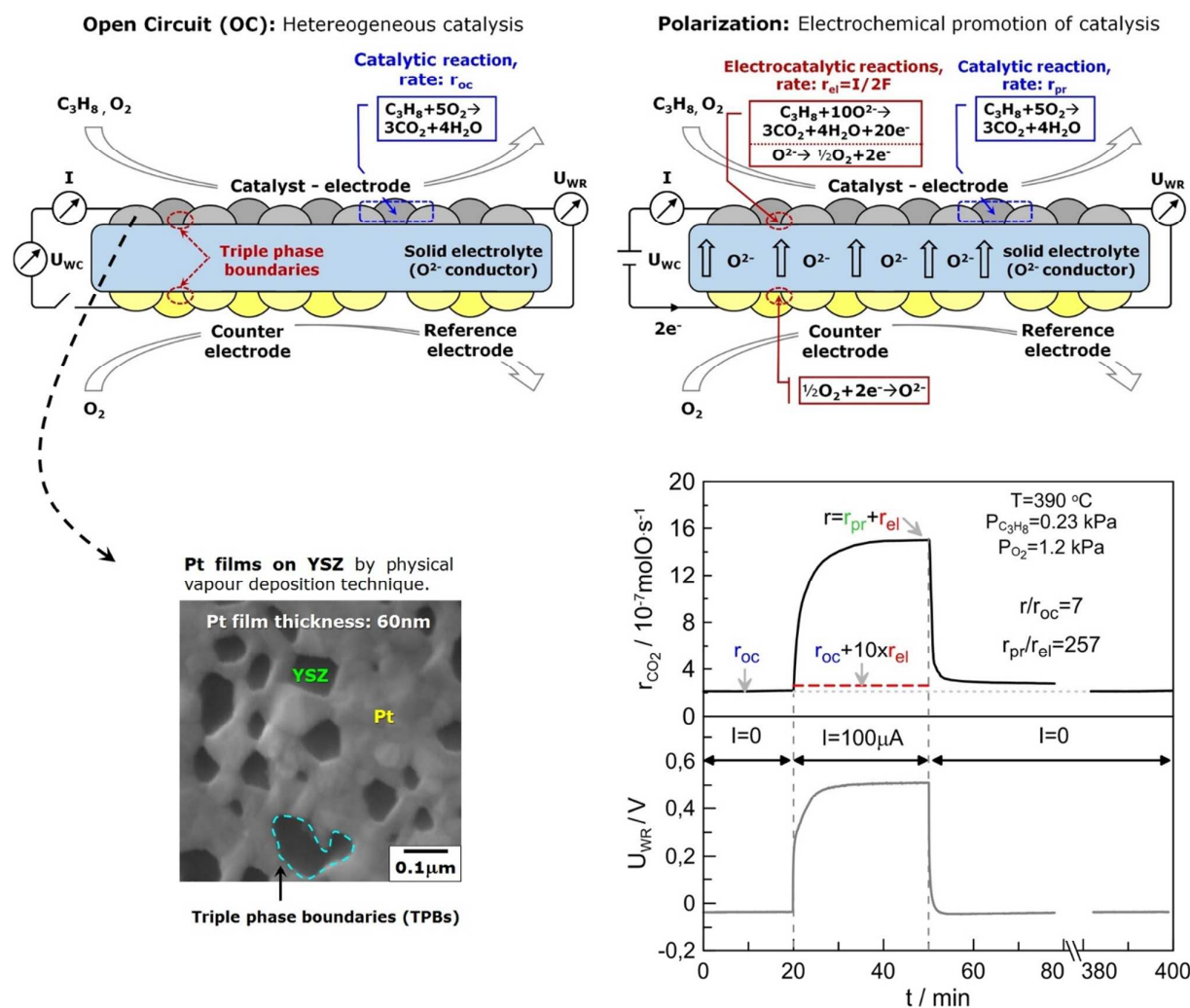
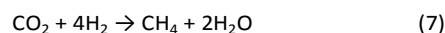
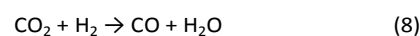


**Figure 2:** (Top) Experimental setup and operating principle of EPOC with  $\text{O}^{2-}$  conducting supports for propane oxidation. (Bottom-Left) SEM image of the Pt porous electrode film deposited by physical vapour deposition technique. (Bottom-Right) Catalytic rate,  $r$ , response of propane oxidation on Pt deposited on YSZ (an  $\text{O}^{2-}$  conductor) upon step change in applied current. The catalyst-electrode potential,  $U_{WR}$ , response with respect to the reference electrode (R) is also shown with the grey line. Reprinted from ref. 20 with the permission of Elsevier.

Electrochemical promotion can affect not only catalytic activity but more importantly product selectivity. An example is shown in figure 3 for the case of  $\text{CO}_2$  hydrogenation on Ru/YSZ<sup>23</sup>. One observes that increasing catalyst potential,  $U_{WR}$ , causes a 4-fold increase in the rate of  $\text{CO}_2$  methanation:



and at the same time a 2-fold decrease in the rate of the competing reverse water-gas shift reaction (RWGS):



The selectivity to  $\text{CH}_4$  increases from 42% without polarization to 82% upon application of  $150 \mu\text{A}/\text{cm}^2$  (i.e.  $U_{WR} = 1.3\text{V}$ ).

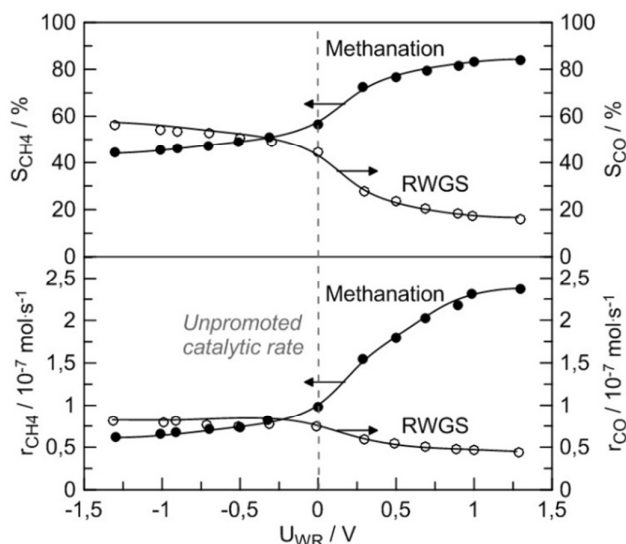


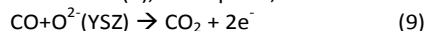
**Figure 3:** Effect of catalyst potential,  $U_{WR}$ , to (top) the product selectivity and (bottom) rate of the methanation and the competing RWGS reaction during EPOC of  $\text{CO}_2$  hydrogenation on Ru/YSZ.  $P_{\text{H}_2}=7\text{kPa}$ ,  $P_{\text{CO}_2}=1\text{kPa}$ ,  $T=220^\circ\text{C}$ . Reprinted with permission from ref. 23. Copyright, 2012, American Chemical Society.

## 2.2. Physicochemical origins of EPOC: The assumption of the sacrificial promoter mechanism

As shown schematically in figure 4 for the case of CO oxidation, when oxygen ions ( $\text{O}^{2-}$ ) are arriving at the three-phase boundaries catalyst/solid electrolyte/gas under the influence of a positive current or potential, from there adsorbed species which have only three possibilities (scenarios 1-3):

- Desorption to the gas phase,
- Reaction with a coadsorbed species,
- Migration over the entire gas-exposed catalyst electrode surface (spillover) followed by possible desorption or reaction with coadsorbed species.

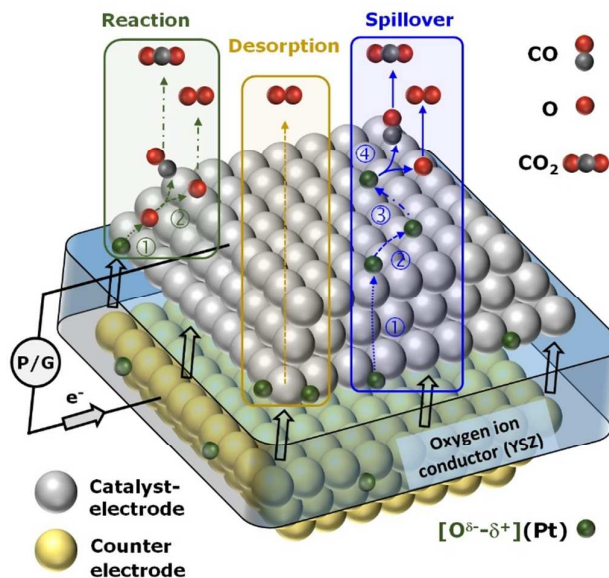
If the electrochemical reactions are fast then the case (a) and (b) will be favored. In case (a) the catalytic rate will be not affected by the polarization. In case (b) ionic species can either react with adsorbed oxygen or CO. When the latter, i.e. electrochemical oxidation of CO (9), takes place,



the rate will proportionally increase with the current intensity, according to the Faraday's law (1).

On the other hand, if the electrochemical processes are quite slow (scenario 3), then the lifetime of ionic species will be increased. In this case the electrode kinetics (3) is so slow that intermediate products such as partially discharged  $\text{O}^{\delta-}$  ionic species can migrate over the entire gas-exposed catalyst-electrode surface (spillover). This situation can only occur when the kinetic of electrochemical reactions such as (3) and (9) are slow, i.e. at low temperatures (below  $500^\circ\text{C}$ ) and for polarizable catalyst-electrode. In addition, it has been experimentally proven that the lifetime of these  $\text{O}^{\delta-}$  ionic

species is long enough to act as promoters if the catalyst surface is already fully covered with "normal" chemisorbed oxygen coming from the gas phase. In that case, ionic species introduced electrochemically onto the catalyst surface can interact with coadsorbed reactants. These ionic species create a local electrostatic field that can modify the electronic properties of the catalyst and then its chemisorptive properties, and thus change the catalytic properties of the



catalyst surface, which is nevertheless not subject to Faraday's law<sup>6</sup>.

**Figure 4:** Possible pathways of  $[\text{O}^{\delta-}\delta^+](\text{Pt})$  adsorbed species created at the three-phase boundaries via application of electric current: (left) Reaction; (middle) Desorption; (right) Spillover (followed by reaction). Case of the CO oxidation.

Therefore, EPOC is not related to any electrochemical reactions. EPOC has been observed and investigated for more than 80 catalytic reactions, and it is now well established that EPOC is not limited to any particular class of conductive catalysts, solid electrolytes or catalytic reactions<sup>6</sup>. In the case of  $\text{O}^{2-}$  ionic conductors, it has been proposed in the literature by using different techniques such as Temperature-Programmed Desorption (TPD) both in ultra-high vacuum and atmospheric conditions<sup>24-29</sup>, Kelvin probe measurements<sup>30</sup>, XPS<sup>31</sup>, cyclic voltammetry<sup>32</sup>, STM (Scanning Tunneling Microscopy), that the electrochemical supply of  $\text{O}^{2-}$  species on a catalyst surface already nearly saturated with normally adsorbed oxygen (e.g. the well-known  $\text{O}(2\times 2)$  adlattice on Pt(111)) can form a second more ionic and more strongly adsorbed species, denoted  $\text{O}^{\delta-}\delta^+$  (Figure 5). This dipole is overall neutral, as the charge  $\delta^-$  is compensated by the image charge,  $\delta^+$ , in the metal<sup>1,6</sup>. These spillover ionic species can act as a promoter (figure 5) for catalytic oxidations due to its repulsive lateral interactions with normally co-adsorbed oxygen (electron acceptors), and its attractive lateral interactions with co-adsorbed electropositive adsorbates (electron donors such as ethylene). These ionic promoting

## PERSPECTIVES

species form an effective double layer at the metal-gas interface and deeply affect the chemisorptive bond strength of co-adsorbed reactants and catalytic intermediates, thereby causing strong promotion of catalytic activity and selectivity. In addition, the correlation between the modification of catalyst electronic properties and the catalytic rate variation induced by the applied potential has been clearly established by measuring the “in-situ” modification of the catalyst work function<sup>30</sup>. Rules have been established to predict the impact of the polarization on the catalytic activity of a catalyst-electrode according to the nature of the ions and the chemisorptive properties of reactants on the catalyst<sup>1,6</sup>. The EPOC mechanism is called “sacrificial promoter” mechanism because the ionic promoting species can also react with the oxidizable reactant and thus have a finite mean residence time,  $\tau_p$ , on the catalyst surface. This residence time is a factor of  $\Delta$  larger than the residence time,  $\tau_r$ , of the key reactant on the catalyst surface<sup>1,6</sup>.

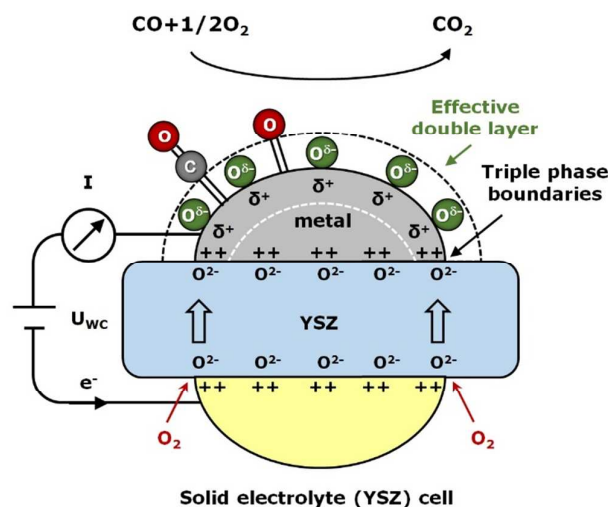


**Figure 5:** Schematic of the “sacrificial promoter” mechanism of EPOC.

As already mentioned, the presence of different oxygen ionic species has been evidenced in the EPOC literature by using many techniques<sup>6</sup>, such as Temperature-Programmed Desorption (TPD) experiments.

TPD investigations under real conditions (i.e. adsorption of oxygen at atmospheric pressure under polarization) were carried out by our group<sup>29</sup>. The catalyst-electrode was a thin and porous Pt film (geometrical area of 24 cm<sup>2</sup>) deposited on a dense YSZ tube. It has been shown that propane combustion can be strongly electropromoted at 400°C upon positive polarizations, as depicted in figure 2. Faradaic efficiency of 52 has been measured upon positive current of +5 mA. To get insights into the origin of this EPOC process, O<sub>2</sub>-TPD experiments have been performed in same operating conditions that used during catalytic activity measurements. First, gas oxygen was adsorbed at 400°C under atmospheric pressure and then the reactor was cooled at 100°C under the same gas mixture. The TPD spectrum was recorded under He

## Catalysis Science &amp; Technology

flow and exhibited only one O<sub>2</sub> desorption peak at 390°C. Interestingly, as shown in figure 6, a second O<sub>2</sub> desorption peak centered at 640°C appeared in the TPD spectrum, when anodic polarization took place during oxygen adsorption at identical conditions. The area of the second peak was increased as the applied current was varied from 1 to 5 mA, thus confirming its relation with ionic oxygen species. However, the most important point is that the first oxygen desorption peak, attributed to “normal” chemisorbed oxygen species, is shifted to lower temperatures. This underlines that the positive polarization enables the formation of weakly adsorbed oxygen species (coming from the gas phase).

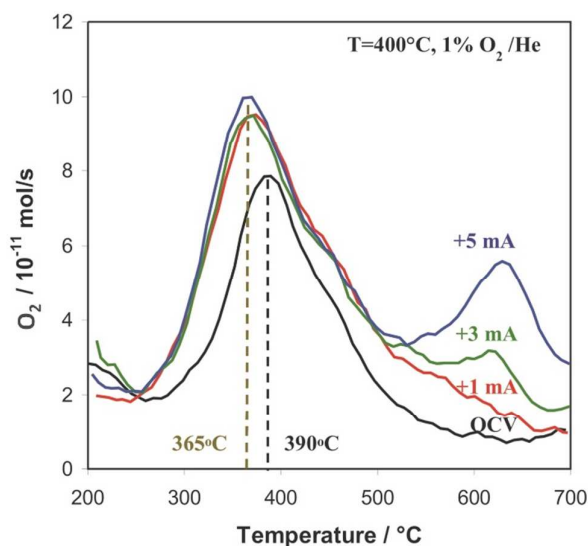
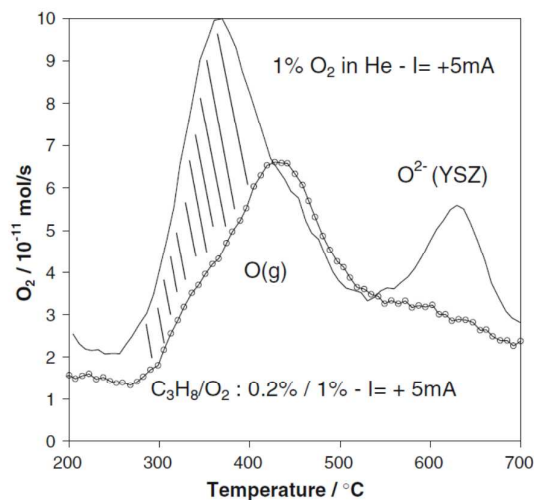


**Figure 6.** Atmospheric pressure O<sub>2</sub>-TPD spectra after oxygen adsorption at 400 °C for 1 h under anodic polarization with different positive currents: +1, +3, and +5 mA. Operating conditions during oxygen adsorption: reactive mixture: O<sub>2</sub> 1% in He; flow rate, 10 L h<sup>-1</sup>. Reprinted from ref. 29, with kind permission from Springer Science and Business Media.

In an additional experiment, oxygen was adsorbed at 400°C for 1 hour under atmospheric pressure and under anodic polarization (+5 mA) while propane was also present in the gas phase (thus catalytic phenomena were taking place). Then the system was cooled at 200°C and the TPD spectra were obtained under He flow. The temperature of 200°C was selected in this experiment in order to minimize the effect of the cooling procedure on the adsorbed species. Figure 7 gives a comparison between the TPD spectra recorded after adsorption of oxygen under anodic polarization in presence and in absence of propane and subsequent cooling down. From the difference between the two spectra, it comes out that propane has reacted with the weakly adsorbed oxygen species induced by the polarization, which are more reactive. Additionally a part of ionic oxygen species has also reacted with propane.

These results clearly showed that anodic polarization generates the migration of backspillover ionic oxygen species from YSZ toward the Pt surface. These species act as

promoters and enable the formation of more reactive chemisorbed oxygen species, thus responsible for the activity enhancement. Therefore, EPOC can be considered as an electrically controlled metal support interaction<sup>29</sup>.



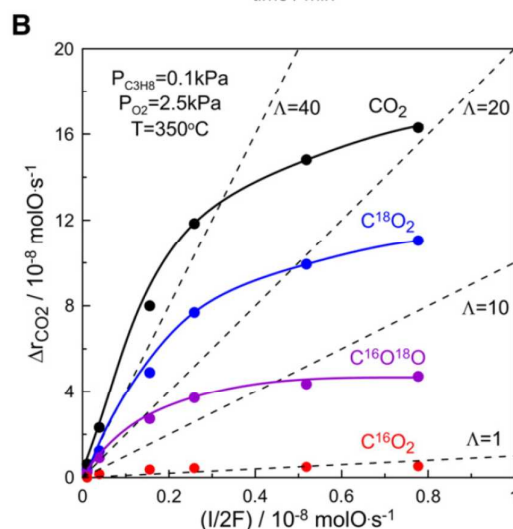
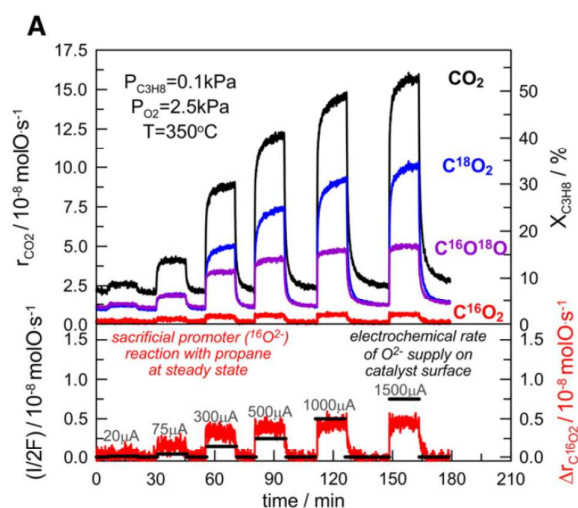
oxygen under anodic polarization (+5 mA) with and without propane. Operating conditions during oxygen adsorption: reactive mixture is  $C_3H_8/O_2$ : 0.2%/1% or 1%  $O_2/He$ , overall flow rate  $10 L h^{-1}$ ,  $T=400^\circ C$ , adsorption for 1 hour. Reprinted from ref. 29, with kind permission from Springer Science and Business Media.

The sacrificial promoter mechanism of EPOC was confirmed recently by Tsampas et al<sup>33</sup>, conducting isotopical labeling experiments during the electrochemical promotion of propane oxidation on Pt/YSZ. The aim of this study was to *operando* distinguish the oxygen species coming from the solid electrolyte with those from the gas phase. A two-compartment tubular electrochemical catalyst with a three-electrode configuration was used. The reaction compartment was exposed to propane and isotopic oxygen ( $^{18}O_2$ ), while the second compartment was supplied with air for replenishing the electrolyte with normal oxygen ( $^{16}O_2$ ). In such configuration, the reaction between propane and the promoting ionic species leads to formation of  $C^{16}O_2$  and the reaction between propane and gas phase oxygen forms  $C^{18}O_2$ . The results of figure 8 is in good agreement with the sacrificial promoter mechanism. Figure 8 shows that propane oxidation can be strongly electropromoted ( $\rho$  values up to 6) upon application of positive polarizations. As shown clearly in figure 8b, significant electropromotion is obtained in the combustion of propane with the gas phase oxygen (production of  $C^{18}O_2$ ). Interestingly, one observes that the increase in the rate of  $C^{16}O_2$  formation practically coincides with the rate  $(I/2F)$  of  $O^{2-}$  supply to the catalyst ( $\Lambda C^{16}O_2=1$ ), thus confirming that the  $C^{16}O_2$  production can only be attributed to the (sub)Faradaic electrochemical oxidation of propane.

Another important feature of the experiment of figure 8 is the production of  $C^{16}O^{18}O$ , which can be attributed to surface oxygen exchange at the triple-phase-boundaries. It appears

that this scrambling between the two oxygen species, generates active oxygen species because no  $^{18}O_2$  was detected in the gas phase and therefore desorbs from the surface. The rate of  $C^{16}O^{18}O$  production (and thus of the oxygen exchange rate) can also be electropromoted as shown in figure 8, but to a lesser extent than that of  $C^{18}O_2$ . The findings of this study suggest that the presence of ionic sacrificial promoting species onto the catalyst surface generates more reactive oxygen species coming from the gas phase, either directly adsorbed on Pt or through the YSZ support<sup>33</sup>.

Figure 8. (A) Catalytic rate responses to step changes of



various applied positive currents during  $C_3H_8$  oxidation on Pt/YSZ. (B) Effect of electrochemical rate of  $O^{2-}$  supply on the  $CO_2$  production rate increase. Dashed lines correspond to Faradaic efficiency values equal to 1, 10, 20, and 40. Reprinted from ref. 33 with the permission of Elsevier.

Similar isotopic labeling experiments were conducted for the investigation of EPOC origins in the case of electropromotion under negative polarization (i.e. oxygen ions are removed from the catalyst). It was found that the negative current application only affects the region near the tpb while (high)

positive current application causes an effect in the overall gas/solid interface<sup>34</sup>.

Although the electrochemically induced spillover of the ionic species onto the metallic catalyst surface has been unambiguously demonstrated, some issues remain on the mechanistic understanding of the EPOC effect. The first opening question remains on the real existence of the strong dipole induced by the backspillover oxygen species. The charge of these latter between -1 and -2 has not yet been clearly determined. There is no doubt that the polarization of the Me/YSZ interface can modify the electronic properties of the metal. The modification of the catalyst work function (WF) is clearly associated with the electrochemically induced spillover of adsorbates. However, it has not been yet clearly proved that this modification of electronic properties is only due to strongly adsorbed ionic species and/or to the effect of the polarization itself. The direct equality between the WF and the applied potential cannot be considered as a general law but is valid for a number of catalytic systems. Using thermodynamic calculations, Metcalfe<sup>35,36</sup> has confirmed this relationship but after considering some specific conditions:

- Application of moderate overpotentials.
- Low lateral interactions between surface ions.
- Fast surface diffusion of ionic species.

EPOC mechanism seems to join theories of the Strong Metal-Support Interaction (SMSI) effects in which electronic interactions are key parameters of the enhanced catalytic activity of metallic nanoparticles dispersed on redox-active oxides. Some studies on the promoted catalytic activity observed on precious metals/ceria catalytic systems after reduction in H<sub>2</sub> have shown a direct link between the work-function of the metal and the reducibility of ceria<sup>37,38</sup>.

A recent study has demonstrated that the d-band center theory can be a more effective electronic descriptor of SMSI<sup>39</sup>. The changes of the d-band centers of metal surfaces based on DFT calculations have been introduced by Hammer and Nørskov<sup>40</sup>. The d-band center is the average energy of electronic d states project on a surface metallic atom. It is considered as a key parameter in the chemisorptive properties of a metallic surface<sup>41</sup>. According to this model, changes in the d-band center, caused for instance by a polarization, create an antibonding state above the Fermi Level. A chemical bond between an adsorbate and the metal is strengthened (weakened) if the antibonding states are shifted up (down) relative to the Fermi level. This d-band center model is not in contradiction with the EPOC rules used to predict the modifications of chemisorptive properties of metallic catalyst according to the WF changes induced by the polarization<sup>1,6</sup>. For instance, considering the adsorption of O<sub>2</sub> on the Pt/YSZ electrochemical catalyst, EPOC studies have shown that positive polarizations induce an increase in the WF which provokes a weakening of the Pt-O chemical bond, as experimentally observed<sup>6,29</sup>. The increase of the WF implies a shift down of the Fermi level, as similar as the shift down of the antibonding states relative to the Fermi level. Nevertheless, DFT calculations could be very useful to

calculate the change in d-band centers of metal surface interfaced on a solid electrolyte upon polarization.

### 3. YSZ as catalytic support

#### 3.1. Metal Support Interactions

It is well established in the field of Heterogeneous Catalysis that some oxide supports, such as ceria or titania, except from providing high dispersion and surface area for the catalyst, have also an active role in the catalytic mechanism. This effect of support on catalytic activity or selectivity was called in the literature as Metal Support Interactions (MSI)<sup>1,6,42-44</sup>, known as Schwab effect of the second kind (Schwab effect of the first kind refers to the effect of a supported metal on the catalytic properties of a metal oxide)<sup>1,6</sup>.

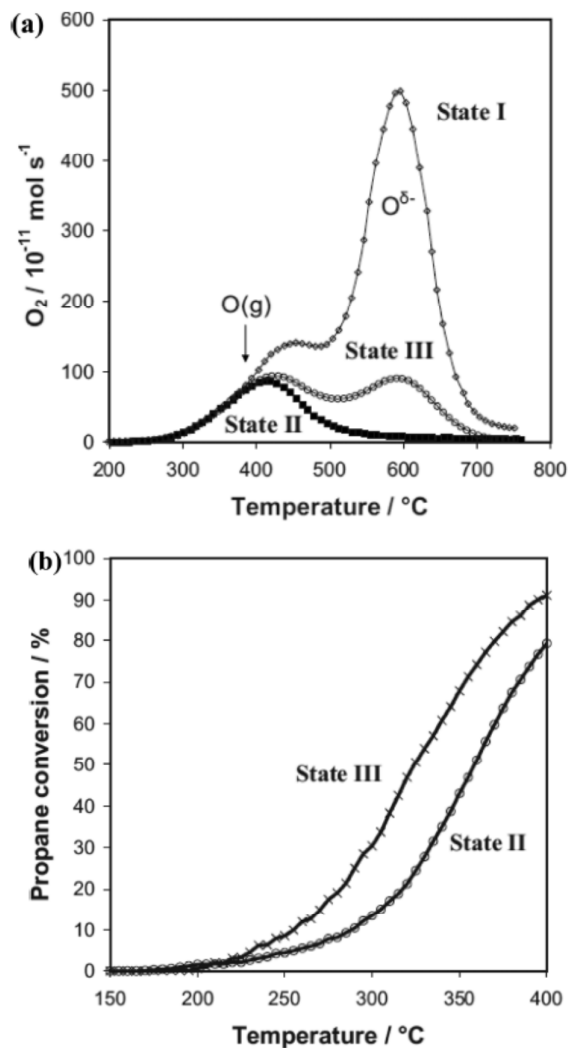
Since the discovery of this effect by Tauster<sup>45</sup>, the origin of the MSI is still not fully clarified. The oxygen vacancies in the support (e.g. YSZ) have been credited to be responsible for the MSI effect. It has been also proposed that metal particles are decorated by oxygen ions (O<sup>2-</sup>) and these ions participate on the chemisorptive properties of the catalysts<sup>1,6,46-48</sup>. Various studies have compared the magnitude of MSI with that of EPOC and demonstrated that these two phenomena can be explained by a similar process, which is the backspillover of O<sup>2-</sup> ionic species onto the metallic particles<sup>49-53</sup>. For instance, our group<sup>53</sup> has investigated the effect of O<sup>2-</sup> ionic species on the catalytic performance of Pt nanoparticles supported on YSZ (under various thermal treatments) for propane deep oxidation. Representative results of this study are shown in Figure 9.

Figure 9a shows the O<sub>2</sub>-TPD spectra recorded after adsorption of oxygen for 1h at:

- (i) 300 °C on the fresh Pt/YSZ-supported catalyst (denoted as state I),
- (ii) 300 °C on the Pt/YSZ-supported catalyst after the first TPD (denoted as state II), and
- (iii) 500 °C on the Pt/YSZ-supported catalyst after the second TPD (denoted as state III).

Two distinct oxygen desorption peaks are present in the TPD spectra at states I and III, demonstrating the coexistence of two different binding strengths of chemisorbed oxygen on the Pt surface, suggesting two O adsorption states<sup>53</sup>. As already mentioned in paragraph 2.2 of this article, similar results have been obtained during TPD investigations of the EPOC origins<sup>24-29</sup>, where the first peak has been attributed to gaseous chemisorbed oxygen and the second one to the migration of oxygen ionic species from the YSZ bulk. After the first TPD, no more nonstoichiometric oxygen species existed in the bulk (YSZ was practically depleted), thus the migration of ionic species became impossible. This explains the fact that only one peak was observed in the TPD spectrum at state II (Figure 8a). Finally, during the pretreatment at 500 °C under oxygen (state III), the YSZ bulk was partially replenished and thus the second peak appeared in the third TPD spectrum<sup>53</sup>. The catalytic performance of propane deep oxidation with Pt/YSZ catalysts at states II and III is presented in figure 9b. Higher catalytic activity of state III-catalyst was observed above 220 °C. As in

both states II and III, the Pt dispersion is the same (13%), the only difference between the two catalysts was their ability to induce thermal migration of  $O^{2-}$  species from YSZ. This confirms that  $O^{2-}$  ionic species can effectively promote alkane deep oxidation at the nanoscale. Thus, figure 9b suggests that the thermally induced migration of  $O^{2-}$  ionic species from YSZ to the Pt surface can strongly promote the propane combustion<sup>53</sup>. These results are in agreement with findings of EPOC investigations, where it was found that positive current



application, which causes the migration of lattice  $O^{2-}$  species (by electrochemical pumping) toward the Pt surface, can enhance the catalytic activity of a Pt/YSZ electrochemical catalyst during propane oxidation at 390°C<sup>1</sup>.

**Figure 9:** (a) O<sub>2</sub>-TPD spectra recorded after adsorption of oxygen on the Pt/YSZ powder catalyst at states I, II, and III. (b) Comparison of the catalytic activity for propane combustion of Pt/YSZ nanodispersed catalysts at states II and III. Reproduced from ref. 53 by permission of The Electrochemical Society.

It thus appears that EPOC can be induced without any electrical polarization by using nanoparticles of metallic catalysts supported on grains of ionic conducting ceramics (in MSI processes), where a self-driven EPOC mechanism occurs at the nanometric scale.

### 3.2. YSZ as an active catalytic support for oxidation reactions

Other recent works on nanodispersed Pt particles on YSZ confirmed the promoting role of  $O^{2-}$  species on the catalytic oxidation of ethylene<sup>54</sup>, toluene<sup>55</sup> and carbon monoxide<sup>56-58</sup>. Figure 10 gives an example of these studies and compares the catalytic performance during CO oxidation of Pt nanoparticles (with same metal loadings) deposited on different supports<sup>57</sup>. Line (a) refers to Pt nanoparticles supported on YSZ using the wet impregnation method. Lines (b), (c) and (d) correspond to Pt nanoparticles deposited on YSZ,  $\gamma$ -Al<sub>2</sub>O<sub>3</sub> and C supports respectively using the modified polyol reduction preparation method (average Pt size is 1.8-2.8 nm). The catalyst prepared by wet impregnation shows poor catalytic performance compared to the catalysts prepared by the modified polyol method, due to the small Pt nanoparticles with narrow size distribution which appear in the latter case. Comparing the three catalysts prepared by the modified polyol method, the catalytic performance of Pt/YSZ is superior than that of Pt/C and Pt/ $\gamma$ -Al<sub>2</sub>O<sub>3</sub>, despite the fact that the specific surface area of Pt/ $\gamma$ -Al<sub>2</sub>O<sub>3</sub> and Pt/C is 10 and 20 times respectively larger than Pt/YSZ and also that the Pt dispersion is higher on  $\gamma$ -Al<sub>2</sub>O<sub>3</sub> and C compared to YSZ.

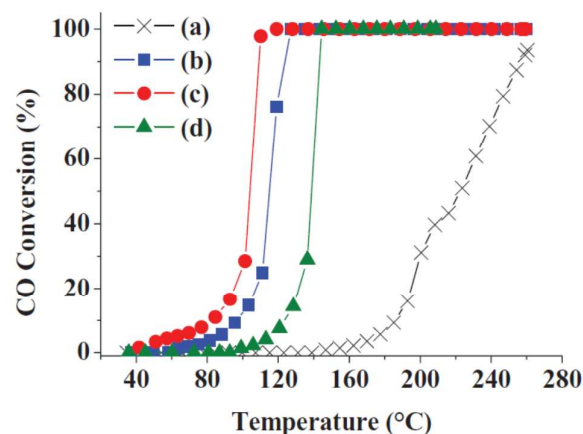


**Figure 10:** Comparison of catalytic performances for CO oxidation of Pt nanoparticles deposited on (a) Pt/YSZ by wet impregnation, (b) Pt/ $\gamma$ -Al<sub>2</sub>O<sub>3</sub>, (c) Pt/YSZ and (d) Pt/C. Samples (b), (c) and (d) were prepared by the modified polyol method. Temperature ramp = 3°C/min. Flowrate = 4.3 L/h, 770 ppm CO and 4.4% O<sub>2</sub>. Reproduced from ref. 57 by permission of The Electrochemical Society.

According to the authors of this study, the superior performance of Pt/YSZ is related with the ionic conductivity of YSZ, while this is not the case for the C and  $\gamma$ -Al<sub>2</sub>O<sub>3</sub> supports. It was thus concluded that the mobility of  $O^{2-}$  ionic species contained in YSZ has a promoting role on the catalytic activity

of Pt for CO oxidation<sup>57</sup>. The assumption of the authors is indeed in agreement with previous EPOC investigations, where the promoting effect (under electrical polarization) of  $O^{2-}$  for CO oxidation over Pt catalytic films interfaced to YSZ membranes was demonstrated<sup>59</sup>. Thus, the higher catalytic activity of Pt/YSZ (line C) could be related to a spillover mechanism of  $O^{2-}$ , of which the driving force is the difference in WF of YSZ and Pt nanoparticles. However, other factors may also account for the difference in activity between the three investigated catalytic systems, such as the different shapes of the nanoparticles<sup>60</sup> or the changes in the position of the d-band of the metallic nanoparticles via interaction with orbitals from the support at the metal-support interface<sup>39</sup>. In-depth investigations are required in order to elucidate the mechanism of the promotion in case of Pt/YSZ.

Recently, the group of Prof. Baranova from the University of Ottawa in Canada has investigated the CO and ethylene deep oxidation on Pt/YSZ nanodispersed catalysts without any oxygen in the feed<sup>60,61</sup>. They have shown that CO and ethylene can be fully oxidized at low temperatures (below 220°C) without any oxygen in the feed, only with lattice YSZ oxygen species. It was calculated that during one catalytic cycle, up to 18% from the total amount of oxygen in the YSZ support participates in the reaction of ethylene oxidation. This value is in good agreement by literature findings suggesting that 18% of the lattice oxygen of YSZ participates in high temperature (900°C) methane oxidation<sup>62</sup>. However, it was found that this fraction drops to only 1% for the case of CO oxidation. The authors related this difference with the stoichiometry of the reactions (one mole of  $O^{2-}$  for CO oxidation vs 6 moles of  $O^{2-}$  for  $C_2H_4$  oxidation). Another interesting result that derived from this study was that the oxidation of CO or  $C_2H_4$  by lattice oxygen from YSZ is a size-sensitive reaction, since the catalytic activity drops dramatically by increasing the Pt particle size from 1.9 nm to 6.7 nm<sup>62</sup>.

Finally, a mechanism for the reactions was proposed based on the formation of local nano-galvanic cells at the Pt/YSZ/gas phase tpbs, where anodic (electrochemical oxidation of CO and  $C_2H_4$ ) and cathodic (surface partial electroreduction of YSZ) processes occur simultaneously but are separated in space. These results support the idea that, using nanodispersed YSZ-supported catalysts, electrochemical reaction can take place at low temperatures.

### 3.3. Isotopic studies for the investigation of the effect of YSZ lattice oxygen on the catalytic propane oxidation

Our group has recently investigated the role of YSZ lattice oxygen species on the catalytic performances of Pt nanoparticles<sup>63</sup>. Propane deep oxidation with isotopic oxygen took place on Pt nanoparticles deposited on YSZ,  $ZrO_2$  (which presents negligible quantity of oxygen vacancies) and  $SiO_2$  (which is considered as an inert support). The impact of the support's oxygen mobility on the mechanism of propane oxidation was investigated. Figure 11 shows the temperature profiles of the products distribution ( $C^{18}O_2$ ,  $C^{18}O^{16}O$ ,  $C^{16}O_2$ ) using two different catalytic systems, i.e. Pt/YSZ and Pt/ $ZrO_2$ . Interestingly, the main reaction product on Pt/YSZ is  $C^{16}O_2$

(figure 11 top), showing that lattice oxygen species have an active role in the oxidation process. In the investigated temperature range,  $C^{18}O_2$  only appears in the products stream at high temperatures and at low concentrations.  $C^{18}O^{16}O$  production was also observed as a result of surface oxygen exchange and its increase at high temperature is coupled with the drop of the  $C^{16}O_2$  concentration. According to TPD findings, the Pt surface is mainly covered by  $^{16}O$  species which hinder the dissociative adsorption of gaseous  $^{18}O_2$  oxygen. These  $^{16}O$  species, which are covered the Pt surface, are consumed by the reaction but they are continuously replenished since  $C^{16}O_2$  remains the predominant product even at 450°C. Therefore, the rate of spillover of  $^{16}O^{2-}$  from the YSZ support onto the Pt surface is faster than the dissociative adsorption process of gas phase oxygen as well as the propane oxidation rate.

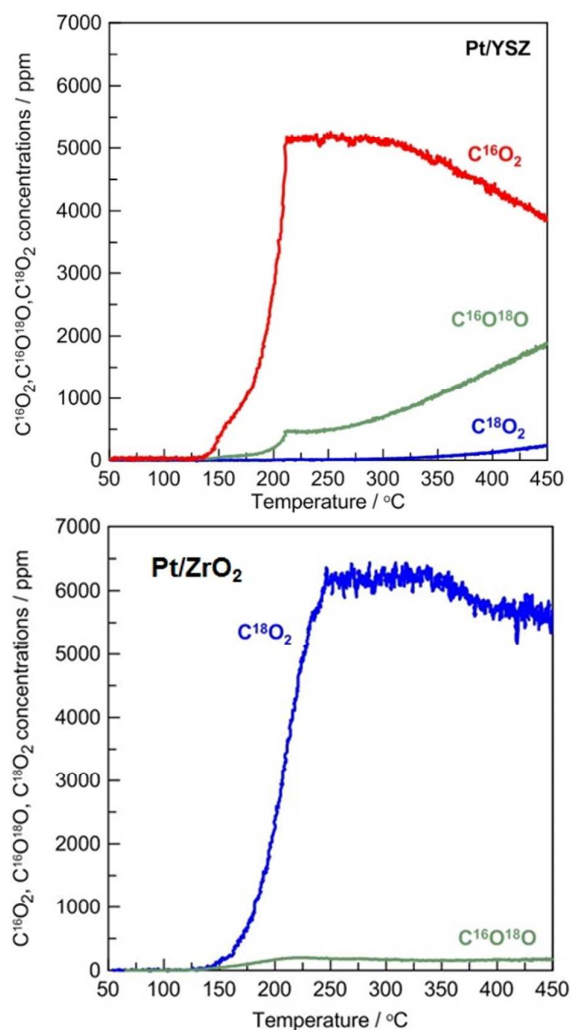


**Figure 11:** Production of the different  $CO_2$  isotopes as a function of the temperature: (blue)  $C^{18}O_2$ ; (green)  $C^{16}O^{18}O$ , (red)  $C^{16}O_2$ . Temperature ramp = 5°C/min, total flow = 1.8 L/h, reaction mixture: 1%  $^{18}O_2$ / 2000 ppm  $C_3H_8$ . (Top) Pt/YSZ, (Bottom) Pt/ $ZrO_2$ . Reproduced from ref. 63 with kind permission from Springer Science and Business Media.

On the other hand, when propane oxidation occurs over Pt/SiO<sub>2</sub> (not shown here) and Pt/ZrO<sub>2</sub> (figure 11 bottom) the product distribution changes completely, since propane predominantly reacts with gas phase oxygen. Therefore, the produced CO<sub>2</sub> is mostly composed by C<sup>18</sup>O<sub>2</sub>.<sup>63</sup>

The results of figure 11 emphasize that, depending on the oxygen mobility in the support, different reaction pathways can take place. These findings can be compared with those presented in figure 8, where EPOC of propane combustion with isotopic oxygen was investigated on Pt films interfaced on dense YSZ membranes. As discussed earlier, positive polarizations can strongly electropromote the C<sup>18</sup>O<sub>2</sub> production (reaction of propane with gas phase oxygen), but not that of C<sup>16</sup>O<sub>2</sub> (oxygen originating from YSZ). The production of C<sup>16</sup>O<sup>18</sup>O is also enhanced in a lesser extent, showing that the oxygen exchange rate is also modified by the polarization.

The results of Figure 11 suggest that the interactions between the Pt nanoparticles and YSZ generate a promoted state similar to that observed upon polarizations during electrochemical promotion of catalysis<sup>63</sup>.

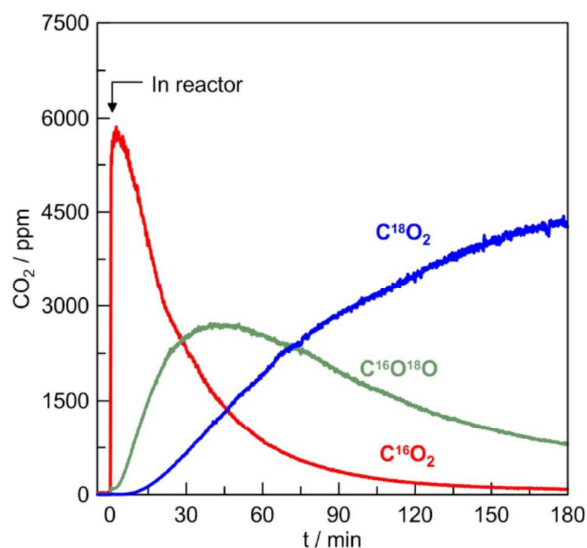


**Figure 12.** Steady-state experiment of propane oxidation by isotopic oxygen. Catalyst Pt/YSZ (loading 1 wt%); T=300°C; Reaction mixture: 1% <sup>18</sup>O<sub>2</sub>, 2000 ppm C<sub>3</sub>H<sub>8</sub>. The arrow shows the moment at which the reaction mixture was provided to the catalyst.

On nanodispersed catalysts, interactions between Pt nanoparticles and the YSZ support are strong and lattice oxygen species are continuously supplied onto the Pt surface, to such an extent that the gas phase oxygen adsorption is strongly inhibited. This lattice oxygen transfer is coupled with the gas phase oxygen incorporation into the YSZ. The situation is very different with EPOC samples since Pt films contain large Pt grains (from 50 nm to more than 1 μm) interfaced on a dense YSZ support. Therefore, the oxygen exchange rate is quite low as well as the lattice oxygen transfer toward the metallic particles. One can consider that the catalytic activity

of the EPOC samples, without any polarization, corresponds to the intrinsic activity of large Pt particles, while the polarization initiates metal-support interactions as observed with nanodispersed catalysts. Therefore, the strong electrochemical promotion of the Pt activity observed in EPOC conditions seems to indicate that the crucial role of the lattice oxygen species observed on nanodispersed Pt/YSZ catalyst could improve the catalytic performances.

Figure 12 displays a steady-state experiment of propane oxidation by isotopic oxygen (at stoichiometric conditions) at 300°C using the Pt/YSZ catalyst. C<sup>16</sup>O<sub>2</sub> is the main product for the first minutes, while after approximately 10 min on stream, the production of C<sup>18</sup>O<sub>2</sub> appears in the gas phase. In parallel, the production of C<sup>16</sup>O<sub>2</sub> gradually decreases with time, as the tank of the YSZ bulk <sup>16</sup>O species is limited. The overall quantity of <sup>16</sup>O involved in the propane oxidation process was calculated (the production of H<sub>2</sub><sup>16</sup>O was estimated taking into account the stoichiometry of the reaction) and found to be in good agreement (with an error margin of 7%) with the initial amount of bulk <sup>16</sup>O atoms inside the sample. It thus appears that all of the YSZ bulk oxygen atoms were involved in the propane oxidation. The results of figure 12 clearly confirm that propane is preferentially oxidized by lattice oxygen species. YSZ has an active role in the reaction since gas phase <sup>18</sup>O species are firstly incorporated inside the YSZ bulk and then react with propane to produce C<sup>18</sup>O<sub>2</sub>. Apart from the cleavage of the C-C and C-H bonds, it seems that Pt nanoparticles also promote the adsorption and desorption of oxygen.

### 3.4. Electrochemically assisted NO<sub>x</sub> storage-reduction catalysts.

Our group in close collaboration with the Laboratory of Synthesis and Functionalization of Ceramics (UMR 3080, CNRS/Saint-Gobain) has recently proposed an innovative catalyst design, inspired from fuel cells, to combine EPOC and high metallic active site availability<sup>64,65</sup>. The design is schematically shown in figure 13, where metallic nanoparticles are dispersed on an O<sup>2-</sup> ionically conducting support, which was deposited into the walls of Diesel Particulate Filter (DPF) made by SiC. The role of the substrate is to provide the electronic conduction in order to ensure the electron transfer between the two different natures of metallic nanoparticles that can be considered as nanoelectrodes (i.e. plays the role of the external electric circuit in the case of EPOC). It was demonstrated that electrochemical effects can improve the catalytic performances of nanodispersed NO<sub>x</sub> storage and reduction (NSR) catalysts deposited in the porosity of SiC mini-DPFs<sup>64</sup>.

The Pt/Rh/YSZ powder catalysts were deposited in the porosity of SiC mini-DPFs. The deposition procedure results in Pt and Rh nanoparticles (Figure 14, right) in the range 2-10 nm, dispersed on YSZ grains (50-100 nm). The average distance between Pt and Rh was less than 10 nm. This configuration simulates an electrochemical cell at nanometric scale. Pt and Rh nanoparticles can be considered as nanometric-electrodes characterized by an asymmetric catalytic behavior in Diesel

## PERSPECTIVES

engine exhausts (which generates an electromotive force), YSZ grain plays the role of the electrolyte and SiC the external circuit in which electrons can flow between the metal nanoparticles (figure 13). Two kinds of SiC materials have been used for the fabrication of mini-DPFs: a conventional non-doped SiC which is an insulator and a N-doped SiC which is an electronic conductor.

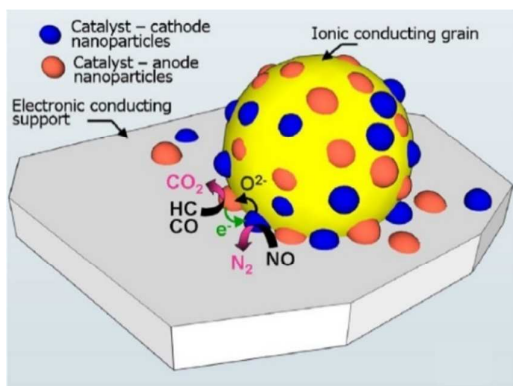


**Figure 13:** Schematic illustration of the electrochemical-assisted NSR catalysts with an  $O^{2-}$  ion conductor (e.g. YSZ) supported washcoat deposited on an electronic conductor SiC-DPF. Reproduced from ref. 64 with permission from Elsevier.

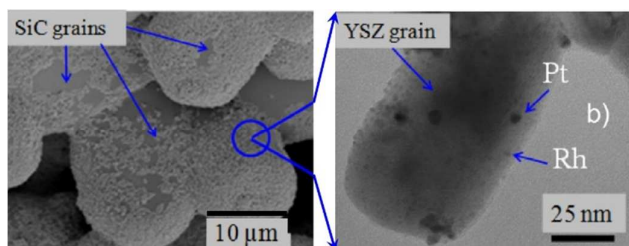
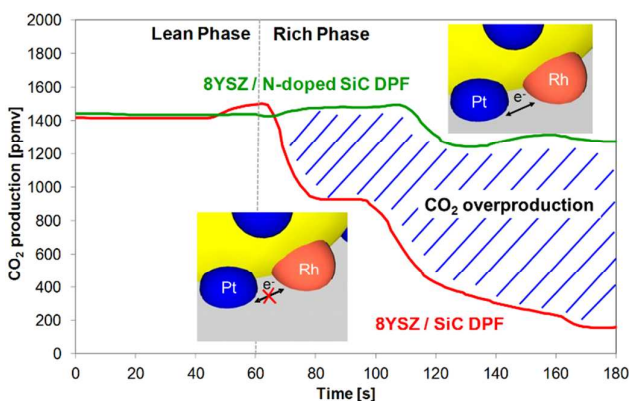


**Figure 14:** Electron microscopy images of Pt/Rh/YSZ nano-cell catalysts supported on SiC-DPF monolith. SEM image (left) of submicronic YSZ particles deposited on the SiC grains of DPF porous wall; zoom (right) on one YSZ grain, observed by HR-TEM, showing individual Pt and Rh nanoparticles at the surface. Reproduced from ref. 64 with permission from



Elsevier.

## Catalysis Science &amp; Technology

**Figure 15:**  $CO_2$  production during lean/rich cycles in Diesel exhaust conditions at  $300^\circ C$  Pt/Rh/YSZ catalysts dispersed on non-doped SiC mini-DPFs and N-doped SiC mini-DPFs. Lean phase, 3 min,  $NO/C_3H_6/O_2/H_2O = 500 \text{ ppmv}/500 \text{ ppmv}/6.5 \text{ vol\%/}10 \text{ vol\%}$ . Rich phase, 2 min,  $NO/C_3H_6 = 500 \text{ ppmv}/500 \text{ ppmv}$ . Overall flow:  $10 \text{ L h}^{-1}$ . Reproduced from ref. 64 with permission from Elsevier.

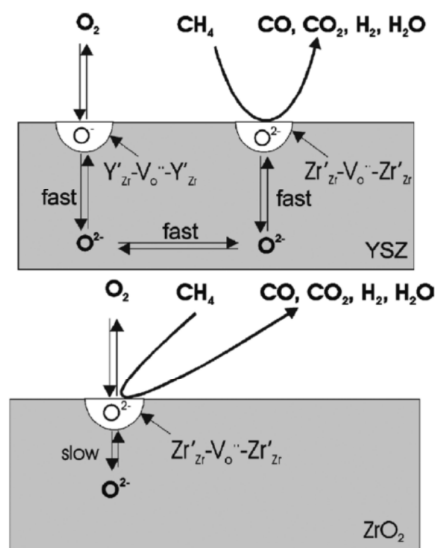
The catalytic performances of these two systems have been evaluated for the  $NO_x$  storage-reduction in cycling conditions (lean/rich). Figure 15 displays the  $CO_2$  production observed during rich cycles (no oxygen, only  $NO$  and  $C_3H_6$ ). A  $CO_2$  overproduction was clearly observed on the catalyst dispersed on N-doped SiC, i.e. when Pt and Rh nano-electrodes are electrically connected. This  $CO_2$  overproduction cannot be accounted by catalytic reactions alone, demonstrating that CO electrochemical reaction is taking place on Pt nanoelectrodes. Conductive SiC materials allow charge transfer to occur, which in turn seems to assist the catalytic processes since the highest catalytic performances have been found on catalysts supported on N-doped SiC.

## 4. YSZ as catalyst for oxidation reactions

### 4.1. Hydrocarbon and CO oxidation

Solid oxides with ionic or mixed ionic-electronic conductivity have been also widely used as catalysts. Their catalytic activity and selectivity have been correlated with their electrical conducting properties, which depend on their crystal and defect structures<sup>66,67</sup>. YSZ has also received attention as a catalyst for several reactions, e.g. total and partial oxidation of methane, oxidation of hydrocarbons and hydrogenation of CO and  $CO_2$ . It has been reported that the vacancies in the crystal lattice of YSZ plays an important role in the reaction and are the catalytic active sites<sup>68-75</sup>.

The Mars-van-Krevelen mechanism<sup>62,69-75</sup> proposed for the catalytic partial oxidation of methane on YSZ is shown in Figure 16. The enhanced catalytic rate of the partial oxidation on methane on YSZ compared to  $ZrO_2$  is related with differences in the defect chemistry between the two oxides. On  $ZrO_2$ , the rate is limited by the rate of re-oxidation of the vacant sites by  $O_2$ . On the other hand, fast diffusion of oxygen in YSZ in conjunction with rapid oxygen activation at extrinsic oxygen vacancies at the surface provides an alternative pathway for replenishment of the oxygen consumed by methane<sup>67</sup>.



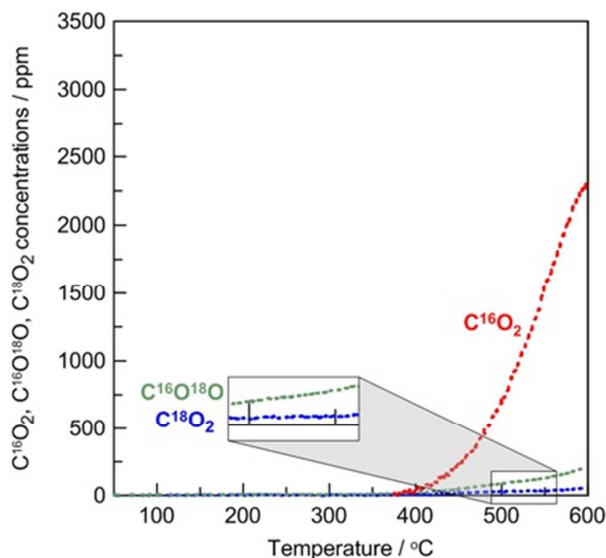


**Figure 16:** Reaction models of the catalytic partial oxidation of methane on YSZ (above) and  $\text{ZrO}_2$  (below) catalysts. Reproduced from ref. 62 with permission from Elsevier.

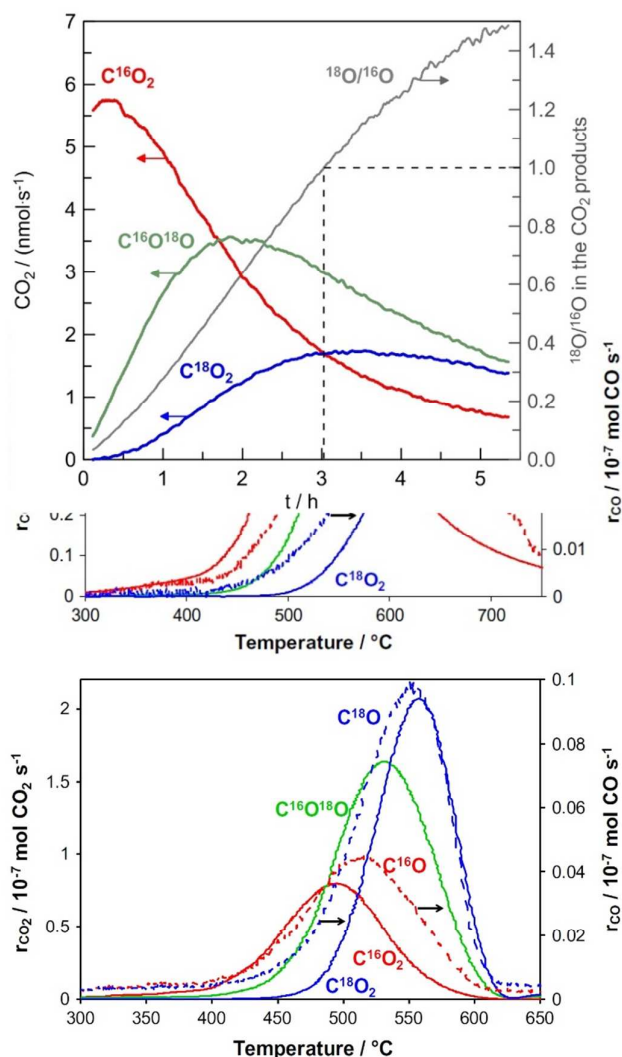
**Figure 17:** Production of the different  $\text{CO}_2$  isotopes during propane oxidation with labelled oxygen on YSZ as a function of the temperature: (blue)  $\text{C}^{18}\text{O}_2$ ; (green)  $\text{C}^{16}\text{O}^{18}\text{O}$ ; (red)  $\text{C}^{16}\text{O}_2$ . Temperature ramp =  $5^\circ\text{C}/\text{min}$ , total flow =  $1.8\text{L}/\text{h}$ , reaction mixture:  $1\%^{18}\text{O}_2/2000\text{ ppm C}_3\text{H}_8$ . Reproduced from ref. 63 with kind permission from Springer Science and Business Media.

In general, the intrinsic catalytic activity of  $\text{O}^{2-}$  conducting solid electrolytes, and of most other ceramics, is much lower than that of metals for most reactions at the same temperature, and thus high temperatures, typically above  $400^\circ\text{C}$ , are necessary to reach practical reaction rate values. This can be clearly seen in figure 11 and 17 which present the temperature profiles of product distribution during propane combustion with isotopic oxygen ( $^{18}\text{O}_2$ ) on YSZ (Figure 17) and on Pt/YSZ (Figure 11a). As one can see, propane oxidation can take place on YSZ in the absence of any metallic active phase. However, the presence of Pt metallic phase on YSZ favors the propane conversion (figure 11a), since the ignition temperature of the reaction was reduced from  $\sim 380^\circ\text{C}$  down to  $\sim 140^\circ\text{C}$ <sup>63</sup>. Another important finding of this experiment is that in both YSZ and Pt/YSZ catalytic systems,  $\text{C}^{16}\text{O}_2$  is the main reaction product, showing that lattice oxygen species are clearly involved in the oxidation process.

#### 4.2. Soot oxidation on YSZ

YSZ has been recently reported as a promising catalyst also for Diesel soot oxidation<sup>76</sup>. Isotopic Temperature-Programmed Oxidation ( $\text{TP}^{18}\text{O}$ ) experiments utilizing labelled oxygen,  $^{18}\text{O}_2$ , demonstrated the key-role of bulk oxygen species in the oxidation process. The experiments were conducted on “tight” soot/YSZ contact mode, which were achieved by soot and YSZ powder mixing and crushing for 15 min in a mortar. Figure 18 presents the profile of soot oxidation products with temperature during temperature programmed oxidation with 1% and 5% of  $^{18}\text{O}_2$ , respectively<sup>76</sup>. The first oxidation products in both cases are  $\text{C}^{16}\text{O}$  and  $\text{C}^{16}\text{O}_2$ , which involve oxygen species originating from YSZ. This implies that oxygen from the gas phase is exchanged during reaction with oxygen from the YSZ lattice.

**Figure 18:**  $\text{CO}$  and  $\text{CO}_2$  production rates as a function of temperature during soot oxidation on YSZ (at “tight” contact mode) with labelled oxygen. Reactant mixture (top) 1% and (bottom) 5%  $^{18}\text{O}_2/\text{He}$ . Reproduced from ref. 76 with permission from Elsevier.



## PERSPECTIVES

## Catalysis Science &amp; Technology

**Figure 19:** CO and CO<sub>2</sub> production rates as a function of time during isothermal soot oxidation on YSZ (at “tight” contact mode) with labelled oxygen at 390°C. Reactant mixture: 5% <sup>18</sup>O<sub>2</sub>/He. Reproduced from ref. 77 with permission from Elsevier.

The production peaks of the different CO and CO<sub>2</sub> products appeared at higher temperatures. When lowering the oxygen partial pressure in the gas phase, the rate of CO<sub>2</sub> production is decreased despite the fact that gaseous oxygen (i.e., <sup>18</sup>O<sub>2</sub>) is not effective to oxidize soot particles below 450°C. This indicates a non-direct impact of the oxygen partial pressure on the soot combustion rate.

Soot combustion with 5% labelled <sup>18</sup>O<sub>2</sub> was carried out isothermally at 390°C (where conversion is below 5%)<sup>77</sup>. Figure 19 presents the product distribution as a function of time. Initially, the main product is C<sup>16</sup>O<sub>2</sub>. The production of C<sup>16</sup>O<sup>18</sup>O linearly increases and then reaches a maximum and decays when the C<sup>18</sup>O<sub>2</sub> production begins. This indicates that the surface oxygen exchange process between gaseous and YSZ oxygen species is effective. As far as one oxygen atom reacts with soot, one is incorporated inside the YSZ.

One can observe the similarities of the CO<sub>2</sub> profiles during isothermal soot oxidation with the case of propane combustion on Pt/YSZ (figure 12). It seems that the underlying mechanism for the oxygen exchange of the gas phase with the oxygen of YSZ bulk under reaction conditions is the same (soot and Pt provide the external circuit for the electrons exchanged during the reaction, respectively). The difference in the time scale between the two experiments is related with the kinetics of the reaction.

Soot oxidation on YSZ involves a fuel-cell type electrochemical mechanism at the nanometric scale schematically presented in figure 20. The efficiency of this electrochemical process seems to depend both on the YSZ/soot contact and on the oxygen partial pressure. Electrochemical oxidation of the soot could occur at the soot/YSZ interface while oxygen electrochemical reaction takes place at soot/gas/YSZ tpbs. Soot particulates could act both as a reactant and a current collector.

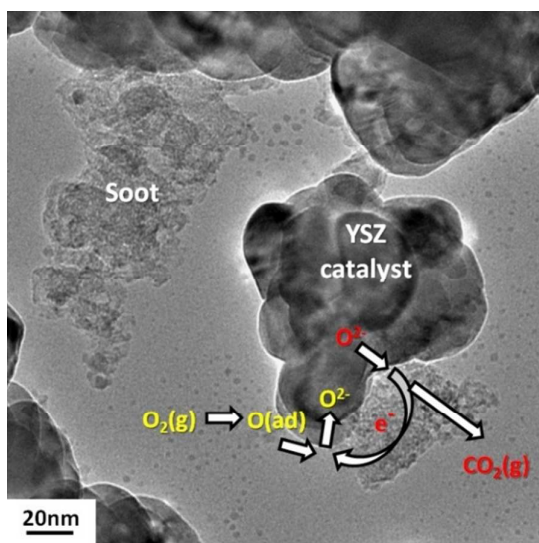
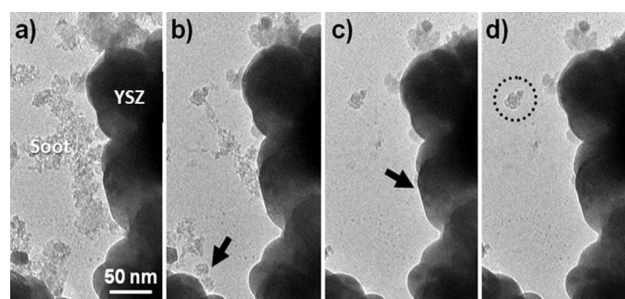


**Figure 20:** ETEM image of soot particulates and YSZ mixture at “tight” contact mode, the soot oxidation mechanism is also schematically presented. Reproduced from ref. 78 with permission from Elsevier.

To get further insights into the mechanism of soot oxidation on YSZ and validate the proposed mechanism, Environmental Transmission Electron Microscopy (ETEM) equipped with an aberration corrector was used for in-situ observations<sup>78</sup>. The resolution of the studies was of around 1 nm. The combustion of a “tight” YSZ/real soot mixture was performed at 550°C in presence of 2-3 mbar of oxygen. Preliminary experiments were conducted to validate that moderate electron beam illumination conditions do not control the soot combustion.

**Figure 21:** Images extracted from video 1 recorded under 3



mbar of O<sub>2</sub> at 550°C. Beam voltage: 80 kV; a) starting time t<sub>0</sub>, b) t<sub>0</sub> + 40s, c) t<sub>0</sub> + 80s, d) t<sub>0</sub> + 120s. Arrows indicate YSZ contact points where the soot particles are consumed. Reproduced from ref. 78 with permission from Elsevier.

Figure 21 depicts the soot oxidation on YSZ and was extracted from a video sequence recorded with an accelerating voltage of only 80 kV at 550°C in presence of 3 mbar of oxygen<sup>78</sup>. Soot particles are agglomerated as grapes with different sizes and shapes. They appear as grey while YSZ crystallites are black. The video sequence clearly evidences that soot grapes are consumed at the interface with the YSZ grains<sup>78</sup>. Small particles got detached from the main assemble during the oxidation, and remained at the proximity of the catalyst on the supporting SiO<sub>2</sub> film, but without any contact with any YSZ particle (circled in Figure 21d). Interestingly, these residues do not get oxidized although entirely surrounded by gaseous oxygen.

Therefore, in-situ ETEM experiments in presence of O<sub>2</sub> confirm that bulk YSZ oxygen atoms are the active species for soot oxidation at the soot/YSZ interface as no oxidation takes place without contact at least under the reasonably moderate electron beam illumination conditions (i.w. 80 kV) used in this study<sup>78</sup>.

Similar to the case of soot oxidation, is the well-known tendency of YSZ to selectively oxidize tar during biomass gasification<sup>79,80</sup>. It has been suggested that the active sites for the tar oxidation are the surface lattice oxygen coordinated with the Zr<sup>4+</sup>-ion, similarly to the case of soot<sup>78</sup> and methane oxidation<sup>63</sup>.

#### 4.3. NO<sub>x</sub> storage capacity of YSZ

A recent study has explored the ability of YSZ to store  $\text{NO}_x^{65}$  in Diesel exhaust conditions. Figure 22a displays the  $\text{NO}_2$  adsorption profile on YSZ at  $250^\circ\text{C}$ , typical temperature of Diesel exhausts. Calculations on the nitrogen balance showed that only part of the total consumed  $\text{NO}_2$  is reduced to NO and consequently an important part of  $\text{NO}_2$  is stored on the YSZ surface. This  $\text{NO}_2$  adsorption is assumed to take place on the YSZ surface oxygen vacancies.

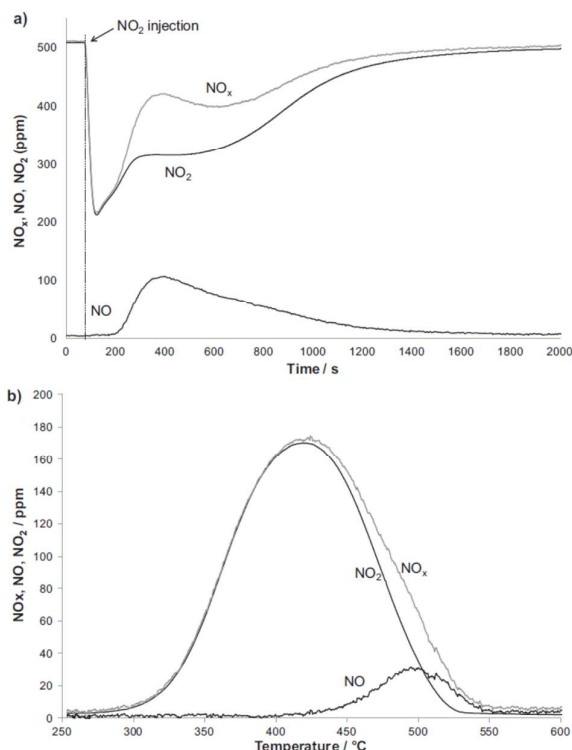


**Figure 22:**  $\text{NO}_x$ ,  $\text{NO}_2$  and NO concentrations as a function of time at  $250^\circ\text{C}$  during (a) the storage and (b) the desorption on YSZ. Storage reactive mixture: 500 ppm  $\text{NO}_2/\text{He}$  ( $10 \text{ l h}^{-1}$ ). Desorption conditions: He,  $10 \text{ l h}^{-1}$ , heating ramp of  $10^\circ\text{C min}^{-1}$ . Reproduced from ref. 65 with permission from Elsevier.

In order to evaluate the nature of the adsorbed species, TPD analysis was carried out under He after  $\text{NO}_2$  adsorption and the results are given in figure 22b. The presence of an intense  $\text{NO}_2$  peak at  $420^\circ\text{C}$  confirms that a significant part of  $\text{NO}_2$  ( $44 \text{ mol/g}_{\text{cat}}$ ) was stored on the YSZ surface during the adsorption step. A comparatively small NO desorption peak ( $4 \text{ mol/g}_{\text{cat}}$ ) is also observed at  $495^\circ\text{C}$  and corresponds to the  $\text{NO}/\text{NO}_2$  thermodynamic equilibrium. This example highlights the interaction of  $\text{NO}_2$  on the YSZ surface. A predominant first step for, at least 2 min before NO production, involves the adsorption of  $\text{NO}_2$  on oxygen vacancies. The second step is initiated 2 min after  $\text{NO}_2$  introduction and is associated with disproportionation of  $\text{NO}_2$  molecules which produce NO release and the formation of zirconium nitrates, nitrites and/or zirconium oxy-nitrates on the weak  $\text{Zr}^{4+}$  basic sites of the YSZ

surface. This process is slow (more than 20 min), suggesting that surface and near subsurface oxygen vacancies are probably involved. Therefore, this study clearly shows the importance of the oxygen vacancies in the  $\text{NO}_x$  adsorption/storage process on the YSZ surface. These punctual defects are able to transform and stabilize the interaction of  $\text{NO}_2$  with the surface oxide, without the presence of a conventional storage component such as BaO or alkaline cation<sup>65</sup>. A recent study has demonstrated the high potentiality of YSZ as a support for NOx storage-reduction catalysts by using high specific surface area YSZ powders prepared from a supercritical  $\text{CO}_2$  process<sup>81</sup>.

A similar recent work based on temperature programmed techniques was carried out by Kauppi et al<sup>82</sup> and it was focused on the interaction of  $\text{H}_2\text{S}$  with  $\text{ZrO}_2$ . This study also highlighted the key role of oxygen vacancies in these interaction; however the results indicate operational differences between the storage of  $\text{NO}_2$  and  $\text{H}_2\text{S}$  on zirconia. According to Kauppi et al<sup>82</sup>, sulphur can be bound on the defect sites of the  $\text{ZrO}_2$  lattice more preferably than oxygen and moreover the sulphur adsorption on the vacancies enhances the reactivity of surface lattice oxygen. Specifically, TPD experiments have indicated that sulphur exchanges with surface oxygen in activated processes based on water formation at two distinct temperatures ( $170^\circ\text{C}$  and  $280^\circ\text{C}$ ). For  $\text{ZrO}_2$ , the surface oxygen sites available for this kind of exchange could be the m-OH (multi-coordinated OH groups), the surface lattice oxygen at terrace sites or the surface lattice oxygen at edges or low-coordination sites. Since the maximal amount of  $\text{H}_2\text{S}$  adsorbed was in the order of 5% of a monolayer, the authors suggested that sulphur replaces oxygen at m-OH at the low temperature ( $170^\circ\text{C}$ ) and surface lattice oxygen at defective sites at high temperatures (up to  $400^\circ\text{C}$ ).

## 5. Concluding remarks - perspectives

This review presents clear evidence that YSZ is a material of growing importance in the field of catalysis. This ceramic is used either as a dense membrane in electrochemical cells or as nanodispersed powders as a support. YSZ combines different functionalities, attractive for heterogeneous processes.

- First, the YSZ surface contains oxygen vacancies. These surface defects can act as active catalytic sites, as demonstrated in the literature for hydrocarbon oxidation or  $\text{NO}_x$  storage. In addition, they can strongly interact with metallic nanoparticles.
- Secondly, these oxygen vacancies are homogeneously distributed into the YSZ crystal lattice, allowing a selective bulk mobility of oxygen ions.

The latter property has been extensively exploited by using YSZ as dense membranes in EPOC processes. This electrochemical activation of catalytic performances is related to the electrochemically supply from YSZ of partially discharged oxygen species on the catalyst surface. These ionic species create a local electrostatic field that can modify the electronic properties of the catalyst and then its chemisorptive properties such as the chemisorption of gaseous oxygen. EPOC can only be observed when the lifetime of these ionic

promoters is high enough. Therefore, EPOC process can only take place when the kinetic of electrochemical reactions is slow (below 500°C) and when the catalyst surface is saturated by “normal” chemisorbed oxygen coming from the gas phase. EPOC is a unique process able to produce ionic promoting species for catalytic reactions and furthermore in an in-situ controlled and predictable manner.

One main issue where further investigations should be focused is related with the identification of the exact nature of the partially discharged ionic species which migrate onto the metallic nanoparticles (e.g.  $O^-$ ,  $O_2^-$ , ...). In-situ investigations with synchrotron or spectroscopic techniques could provide useful insights. Furthermore, DFT calculations could be very promising to calculate the change in d-band centers of metal surface interfaced on a solid electrolyte upon polarization. EPOC represents a quite specific domain of the heterogeneous catalysis, involving low-dispersed catalysts (porous thin films electronically conductors) and a very limited number of interaction between the catalyst and the dense YSZ membrane. The situation is quite different when a high surface specific area YSZ powder supports catalytic nanoparticles. The investigations of the metal/YSZ interactions at the nanoscale during catalytic reactions are few, recent and difficult to carry out as, contrary to EPOC, the charged species migration (ions and electrons) cannot be controlled by an external polarization. Most of these studies, up to present, focus on the interaction between Pt nanoparticles and YSZ for oxidation reactions. The main finding is that YSZ bulk oxygen species are involved in the catalytic mechanism even for temperatures lower than 200°C, via the spillover mechanism of ionic oxygen species from YSZ to the Pt nanoparticles. This underlines the ability of YSZ to chemisorb gaseous oxygen molecules, incorporate them into its lattice as ionic species to finally supply active oxygen species onto the Pt nanoparticles.

Some beneficial effects of using YSZ as the support for Pt catalytic nanoparticles (instead of using inert supports such as  $Al_2O_3$ ) have been evidenced for various oxidation reactions. However, it is still not clear if the oxygen species on Pt nanoparticles, which passed through YSZ, are different and more reactive than those directly chemisorbed on Pt from the gas phase. The key parameter which controls the ionic oxygen species spillover seems to be the driving force induced by oxygen chemical potential gradients between YSZ/gas and YSZ/Pt interfaces.

It is interesting to note that similar effects can be achieved with solid soot/YSZ interfaces as soot is an electronic conductor, as mainly composed of carbon. Therefore, YSZ is a very promising noble metal-free catalyst for oxidizing soot with lattice oxygen species as far as solid soot particles are in contact with the YSZ surface. By using specific operating conditions (no oxygen in the gas feed) or specific catalytic materials (two kinds of metallic nanoparticles supported on YSZ, i.e. Pt and Rh, with different catalytic properties), some studies report indirect evidences that electrochemical reactions, such as CO electrochemical oxidation, can take place at the nanoscale, simultaneously with catalytic chemical reactions. Here also, the synergy between electrochemical and

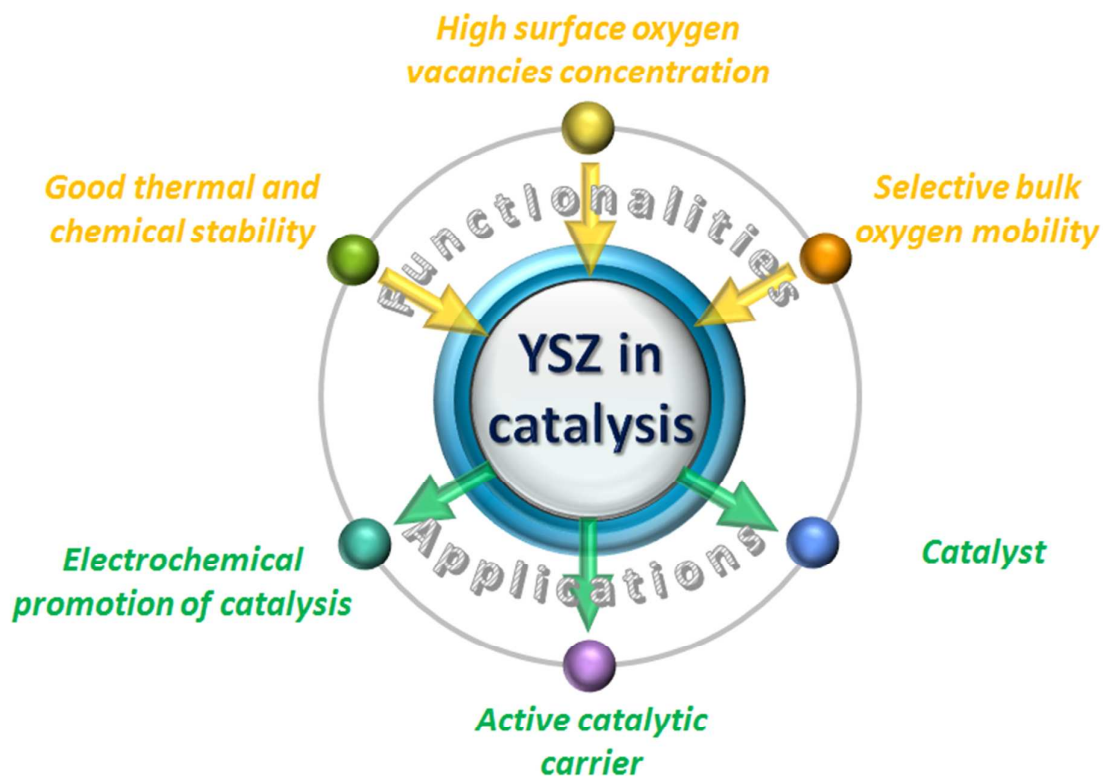
catalytic processes on the same catalytic nanoparticle has not been clearly established.

All these findings emphasize the great potential of YSZ for catalytic applications, mainly for oxidation reactions. These properties together with its good thermal and chemical stability, suggest that YSZ can be the ideal support for the development of smart and efficient catalysts. However, further research is necessary in order to fully understand the interactions between YSZ and metallic nanoparticles.

## References

- 1 P. Vernoux, L. Lizarraga, M.N. Tsampas, F.M. Sapountzi, A. De Lucas-Consuegra, J.L. Valverde, S. Souentie, C.G. Vayenas, D. Tsiplakides, S. Balomenou, E.A. Baranova *Chem. Rev.*, 2013, **113** (10), 8192-8260.
- 2 C. Wagner, *Adv. Catal.*, 1970, **21**, 323-381.
- 3 C.G. Vayenas, H.M. Saltsburg, *J. Catal.*, 1979, **57**, 296-314.
- 4 C. G. Vayenas, B. Lee, J.N. Michaels, *J. Catal.*, 1980, **66**, 36-48.
- 5 R.J. Isaifan, E.A. Baranova, *Electrochem. Commun.*, 2013, **27**, 164-167.
- 6 C.G. Vayenas, S. Bebelis, C. Pliangos, S. Brosda, D. Tsiplakides “Electrochemical activation of catalysis: Promotion, electrochemical promotion and metal-support interactions” Kluwer/Plenum Press, New York, 2001.
- 7 S.J. Skinner, J.A. Kilner, *Materials Today*, 2003, **6** (3), 30-37.
- 8 J.B. Goodenough, *Annu. Rev. Mater. Res.*, 2003, **33**, 91-128.
- 9 H.G. Scott, *J. Mater. Sci.*, 1975, **10**, 1527-1535.
- 10 A.W. Smith, F.W. Meszaros, C.F. Kamata, *J. Am. Ceram. Soc.*, 1966, **49** (5), 240-244.
- 11 K. Kitazawa, R.L. Coble, *J. Am. Ceram. Soc.*, 1974, **57**, 360-363.
- 12 A. Navrotsky, *J. Mater. Chem.*, 2005, **15**, 1883-1890.
- 13 B. Lu, Y.S. Lin, *J. Mater. Sci.* 2011, **46**, 7056-7066.
- 14 L. Malavasi, C.A.J. Fisher, M.S. Islam, *Chem. Soc. Rev.* 2010, **39**, 4370-4387.
- 15 W. Vielstich, A. Lamm, H. Gasteiger “Handbook of fuel cells: Fundamentals technology and applications”, Wiley, New York, 2003.
- 16 C. Lopez-Gandara, F.M. Ramos, A. Cirera, A. Cornet, *Sensor. Actuat. B-Chem.*, 2009, **140**, 432-438.
- 17 C.G. Vayenas, *Catal. Lett.*, 2013, **143**, 1085-1097.
- 18 C.G. Vayenas, *J. Solid State Electrochem.*, 2011, **15**, 1425-1435.
- 19 M. Stoukides, C.G. Vayenas, *J. Catal.*, 1981, **70**, 137-146.
- 20 L. Lizarraga, M. Guth, A. Billard, P. Vernoux, *Catal. Today*, 2010, **157**, 61-65.
- 21 C. Kokkofitis, G. Karagiannakis, M. Stoukides, *Top. Catal.*, 2007, **44**, 361-368.
- 22 N. Kotsionopoulos, S. Bebelis, *Top. Catal.*, 2007, **44**, 379-389.
- 23 D. Theleritis, S. Souentie, A. Siokou, A. Katsaounis, C.G. Vayenas, *ACS Catal.*, 2012, **2**, 770-780.
- 24 S.G. Neophytides, C.G. Vayenas, *J. Phys. Chem.*, 1995, **99**, 17063-17067.
- 25 S.G. Neophytides, D. Tsiplakides, C.G. Vayenas, *J. Catal.*, 1998, **178**, 414-428.
- 26 D. Tsiplakides, C.G. Vayenas, *J. Catal.*, 1999, **185**, 237-251.
- 27 A. Katsaounis, Z. Nikopoulou, X.E. Verykios, C.G. Vayenas, *J. Catal.*, 2004, **222**, 192-206.
- 28 A. Katsaounis, Z. Nikopoulou, X.E. Verykios, C.G. Vayenas, *J. Catal.*, 2004, **226**, 197-209.
- 29 X. Li, F. Gaillard, P. Vernoux, *Top. Catal.*, 2007, **44**, 391-398.
- 30 C.G. Vayenas, S. Bebelis, S. Ladas, *Nature*, 1990, **343**, 625-627.

- 31 S. Ladas, S. Kennou, S. Bebelis, C.G. Vayenas, *J. Phys. Chem.*, 1993, **97**, 8845-8848.
- 32 J. Yi, A. Kaloyannis, C.G. Vayenas, *Electrochim. Acta*, 1993, **38**, 2533-2539.
- 33 M.N. Tsampas, F.M. Sapountzi, A. Boréave, P. Vernoux, *Electrochem. Commun.*, *Electrochem. Commun.*, 2013, **26**, 13-16.
- 34 M.N. Tsampas, F.M. Sapountzi, A. Boréave, P. Vernoux, *Solid State Ionics*, 2014, **262**, 257-261.
- 35 I.S. Metcalfe, *J. Catal.*, 2001, **199**, 247-258.
- 36 I.S. Metcalfe, *J. Catal.*, 2001, **199**, 259-272.
- 37 J. Frost, *Nature*, 1988, **334**, 577-580.
- 38 N. Acerbi, S.C. Tsang, S. Golunski, P. Colliern *Chem. Commun.*, 2008, **13**, 1578-1580.
- 39 N. Acerbi, S.C. Edman Tsang, G. Jones, S. Golunski, P. Collier, *Angew. Chem. Int. Ed.*, 2013, **52**, 7737-7741.
- 40 B. Hammer and J.K. Norskov, *Adv. Catal.*, 2000, **45**, 71-129.
- 41 H. Xin, A. Vojvodic, J. Voss, J.K. Norskov, F. Abild-Pedersen, *Physical Review B*, 2014, **89**, 115114-115118.
- 42 M.C.J. Bradford, M.A. Vannice, *Catal. Today*, 1999, **50**, 87-96.
- 43 D.G. Barton, M. Shtein, R.D. Wilson, S.L. Soled, E.J. Iglesia, *Phys. Chem. B*, 1999, **103**, 630-640.
- 44 C. Linsmeier, E. Taglauer, *Appl. Catal. A*, 2011, **391**, 175-186.
- 45 S.J. Tauster, S.C. Fung, *J. Catal.*, 1978, **55**, 29-35.
- 46 T. Ioannides, X.E. Verykios, *J. Catal.*, 1993, **140**, 353-369.
- 47 T. Ioannides, X.E. Verykios, *J. Catal.*, 1993, **143**, 175-186.
- 48 T. Ioannides, X.E. Verykios, *J. Catal.*, 1994, **145**, 479-490.
- 49 D. Tsiplakides, J. Nicole, C.G. Vayenas, Ch. Comninellis, *J. Electrochem. Soc.*, 1998, **145**, 905-908.
- 50 E. Varkarakis, J. Nicole, E. Plattner, Ch. Comninellis, C.G. Vayenas, *J. Appl. Electrochem.*, 1995, **25**, 978-981.
- 51 J. Nicole, D. Tsiplakides, S. Wodiunig, Ch. Comninellis, *J. Electrochem. Soc.*, 1997, **144**, L312-L314.
- 52 J. Nicole, D. Tsiplakides, C. Pliangos, X.E. Verykios, Ch. Comninellis, C.G. Vayenas, *J. Catal.*, 2001, **204**, 23-34.
- 53 P. Vernoux, M. Guth, X. Li, *Electrochem. Solid State Lett.*, 2009, **12**, E9-E11.
- 54 R.J. Isaifan, E.A. Baranova, *Catal. Today*, **241**, 107-113.
- 55 H.A.E. Dole, R.J. Isaifan, F.M. Sapountzi, L. Lizarraga, D. Aubert, A. Princivalle, P. Vernoux, E.A. Baranova, *Catal. Lett.*, 2013, **143** (10), 996-1002.
- 56 H.A.E. Dole, J.M. Kima, L. Lizarraga, P. Vernoux, E.A. Baranova, *ECS Trans.*, 2012, **45** (1) 265-274.
- 57 R.J. Isaifan, H.A.E. Dole, E. Obeid, L. Lizarraga, P. Vernoux, E.A. Baranova, *Electrochem. Solid State Lett.*, 2012, **15** (3), E14-E17.
- 58 R.J. Isaifan, H.A.E. Dole, E. Obeid, L. Lizarraga, E.A. Baranova, P. Vernoux, *Electrochem. ECS Trans.*, 2011, **35** (28) 43-57.
- 59 M.N. Tsampas, F.M. Sapountzi, C.G. Vayenas, *Catal. Today*, 2009, **146**, 3-4, 351-358.
- 60 R.J. Isaifan, E. A. Baranova, *Electrochem. Commun.* 2013, **27**, 164-167.
- 61 R.J. Isaifan, S. Ntais, M. Couillard, E.A. Baranova, *J.Catal.*, 2015, **324**, 32-40.
- 62 J. Zhu, J.G. van Ommen, H.J.M. Bouwmeester, L. Lefferts, *J. Catal.*, 2005, **233**, 434-441.
- 63 M. Alves Fortunato, A. Princivalle, C. Capdeillayre, N. Petigny, C. Tardivat, C. Guizard, M.N. Tsampas, F.M. Sapountzi, P. Vernoux, *Top. Catal.*, 2014, **57**, 1277-1286.
- 64 W.Y. Hernandez, A. Hadjar, A. Giroir-Fendler, P. Andy, A. Princivalle, M. Klotz, A. Marouf, C. Guizard, C. Tardivat, C. Viazzi, P. Vernoux, *Catal. Today*, 2015, **241**, 143-150.
- 65 W.Y. Hernandez, A. Hadjar, M. Klotz, J. Leloup, A. Princivalle, C. Tardivat, C. Guizard, P. Vernoux, *Appl. Catal. B*, 2013, **130-131**, 54-64.
- 66 P.J. Gellings, H.J.M. Bouwmeester, *Catal. Today*, 1992, **12**, 1-105.
- 67 P.J. Gellings, H.J.M. Bouwmeester, *Catal. Today*, 2000, **58**, 1-53.
- 68 A.G. Steghuis, J.G. van Ommen, K. Seshan, J.A. Lercher, *Stud. Surf. Sci. Catal.*, 1997, **107**, 403-408.
- 69 A.G. Steghuis, J.G. van Ommen, J.A. Lercher, *Catal. Today*, 1998, **46**, 91-97.
- 70 J. Zhu, J.G. van Ommen, A. Knoester, L. Lefferts, *J. Catal.*, 2005, **230**, 291-300.
- 71 J. Zhu, M.S.M Rahuman, J.G. van Ommen, L. Lefferts, *Appl. Catal. A*, 2004, **259**, 95-100.
- 72 M. Labaki, S. Siffert, J.F. Lamonier, E.A. Zhilinskaya, A. Aboukais, *Appl. Catal. A*, 2003, **43**, 261-271.
- 73 M.Y. He, J. Ekerdt, *J. Catal.*, 1984, **87**, 238-254.
- 74 N.B. Jackson, J.G. Ekerdt, *J. Catal.*, 1990, **126**, 31-45.
- 75 N.B. Jackson, J.G. Ekerdt, *J. Catal.*, 1990, **126**, 46-56.
- 76 E. Obeid, L. Lizarraga, M.N. Tsampas, A. Cordier, A. Boréave, M.C. Steil, P. Vernoux, *J. Catal.*, 2014, **309**, 87-96.
- 77 E. Obeid, M.N. Tsampas, S. Jonet, A. Boréave, L. Burel, M.C. Steil, G. Blanchard, K. Pajot, P. Vernoux, M. Tsampas, *Solid State Ionics*, 2014, **262**, 253-256.
- 78 A. Serve, T. Epicier, M. Aouine, F.J. Cadete Santos Aires, E. Obeid, M. Tsampas, K. Pajot, P. Vernoux, *Appl. Catal. A*, 2015, <http://dx.doi.org/10.1016/j.apcata.2015.02.030>
- 79 H. Rönkkönen, P. Simell, M. Reinikainen, O. Krause, *Top. Catal.* 2009, **52**, 1070-1078.
- 80 H. Rönkkönen, P. Simell, M. Niemelä, O. Krause, *Fuel Process. Technol.*, 2011, **92**, 1881-1889
- 81 M. Klotz, W.Y. Hernández, C. Guizard, C. Viazzi, A. Hertz, F. Charton, C. Tardivat, P. Vernoux, *Catal. Sci. Technol.*, 2015, **5**, 2125.
- 82 E.I. Kauppi, J.M. Kanervo, J. Lehtonen, L. Lefferts, *Appl. Catal. B*, 2015, **164**, 360-370.



The main applications of Yttria Stabilized Zirconia in catalysis are briefly reviewed and analyzed based on its functionalities.